

# Statistically-Guided Dual-Domain Meta-Learning with Adaptive Multi-Prototype Aggregation for Distributed Fiber Optic Sensing

Yifan He<sup>a</sup>, Haodong Zhang<sup>b</sup>, Qiuhe Song<sup>c</sup>, Lin Lei<sup>a</sup>, Zhenxuan Zeng<sup>d</sup>, Haoyang He<sup>a</sup>, Hongyan Wu<sup>a,\*</sup>

<sup>a</sup>College of Smart Materials and Future Energy, Fiber-Optic Research Center, Fudan University, Shanghai 200433, China

<sup>b</sup>School of Software, Northwestern Polytechnical University, Xi'an 710129, China

<sup>c</sup>Sichuan Fujinan Technology Co., Ltd., Chengdu 611400, China

<sup>d</sup>School of Computer Science, Northwestern Polytechnical University, Xi'an 710129, China

## Abstract

Distributed Fiber Optic Sensing (DFOS) is promising for long-range perimeter security, yet practical deployment faces three key obstacles: severe cross-deployment domain shift, scarce or unavailable labels at new sites, and limited within-class coverage even in source deployments. We propose DUPLÉ, a prototype-based meta-learning framework tailored for cross-deployment DFOS recognition. The core idea is to jointly exploit complementary time- and frequency-domain cues and adapt class representations to sample-specific statistics: (i) a dual-domain learner constructs multi-prototype class representations to cover intra-class heterogeneity; (ii) a lightweight statistical guidance mechanism estimates the reliability of each domain from raw signal statistics; and (iii) a query-adaptive aggregation strategy selects and combines the most relevant prototypes for each query. Extensive experiments on two real-world cross-deployment benchmarks demonstrate consistent improvements over strong deep learning and meta-learning baselines, achieving more accurate and stable recognition under label-scarce target deployments.

**Keywords:** Distributed Fiber Optic Sensing, Domain Generalization, Meta-Learning, Cross-Domain Recognition

## 1. Introduction

Fiber-optic sensing acquires continuous measurements of strain, vibration, and temperature along tens of kilometers of cable by interrogating minute variations in the optical field. It delivers meter-scale spatial resolution and high temporal sampling while avoiding any distributed active electronics along the route (Rao et al., 2021; Hartog, 2017; Wang et al., 2020). Owing to its long reach, continuous coverage, immunity to electromagnetic interference, and reuse of existing telecom fiber, the technology is broadly applicable to pipeline inspection, power- and railway-corridor monitoring, structural-health and geotechnical monitoring, and environmental and seismic sensing. In perimeter security in particular, a single fiber can provide covert, privacy-preserving continuous coverage, eliminating the need to deploy and maintain dense arrays of point sensors (Muñoz and Soto, 2022; Ajo-Franklin et al., 2019; Lindsey et al., 2019; Tejedor et al., 2019; Zhong et al., 2025).

Current approaches for identifying fiber optic signals range from hand-crafted features using traditional classifiers to end-to-end neural networks. The former extracts time- and frequency-domain descriptors (such as statistical moments, short-time

Fourier transforms, or wavelet coefficients) and performs classification using support vector machines (SVMs), random forests, or hidden Markov models (HMMs) (He and Liu, 2021; Tejedor et al., 2019). The latter uses one- or two-dimensional CNNs or recurrent architectures to learn discriminative representations directly from the raw data stream (Wu et al., 2019a, 2021). While these methods are effective in fixed settings, they fail to generalize reliably across deployments. Differences in fiber type and layout (e.g., underground or wall-mounted), coupling conditions, and ambient noise can lead to significant domain shift (Muñoz and Soto, 2022). New sites often provide little or no labeled data, and even source deployments may lack sufficient within-class coverage to capture the diverse patterns of activity. As a result, models overfit to the training conditions and experience a sharp decline in performance when moved to new locations.

A natural response is to seek domain generalization. Conventional domain adaptation or transfer learning improves robustness when some target-domain data (unlabeled or a few labels) are available for fine-tuning or distribution alignment; however, such data are frequently unavailable or costly to obtain in perimeter security deployments. In contrast, meta-learning offers an attractive fit for this problem: by training episodically across multiple deployments, with support/query splits that mimic cross-deployment testing, the learner acquires task-level adaptation skills that transfer to unseen sites without target labels (Finn et al., 2017; Snell et al., 2017; Ye et al., 2020). Meta-learning also naturally supports few-shot and low-data regimes, aligning with the realities of field deployment and the variability intrinsic to interferometric fiber signals (Luong et al., 2023).

\*Corresponding author. E-mail: hywu@fudan.edu.cn

Email addresses: yfhe25@m.fudan.edu.cn (Yifan He), zhang\_haodong@mail.nwpu.edu.cn (Haodong Zhang), qhsong@fudan.edu.cn (Qiuhe Song), leilin0603@163.com (Lin Lei), zengzhenxuan@mail.nwpu.edu.cn (Zhenxuan Zeng), hyhe25@m.fudan.edu.cn (Haoyang He), hywu@fudan.edu.cn (Hongyan Wu)

Despite this promise, three gaps remain in applying meta-learning to fiber-optic sensing: (i) Missing dual-domain synergy under multimodality. Existing models typically emphasize either time-domain or frequency-domain features, or fuse them with static rules (Zhang et al., 2022). They also often assume a single prototype per class, which cannot cover the multi-modal patterns that arise across deployments and coupling conditions. A principled time+frequency collaborative meta-learner with multi-prototype class representations and a sound fusion rule is needed (Zhang et al., 2022; Allen et al., 2019). (ii) Lack of statistical guidance to coordinate views. The relative reliability of time vs. frequency evidence varies by sample and deployment (e.g., SNR, noise color, bandwidth) (Titov et al., 2022). Current methods rarely exploit raw statistical descriptors to infer domain importance or prototype sensitivity, leaving fusion under-informed. (iii) No query-adaptive decision at inference. Most meta-classifiers compare a query to fixed class prototypes; they do not adapt the class representation per query. For interferometric signals with localized artifacts and variable coupling, the classifier should select and weight the most relevant prototypes conditioned on the query’s own statistics (Ye et al., 2020; Vinyals et al., 2016).

We address these gaps with Statistically-Guided Dual-Domain Meta-Learning with Adaptive Multi-Prototype Aggregation, a framework tailored for cross-deployment fiber-optic sensing with Michelson-based vibration capture. Our contributions are threefold:

- We design a dual-domain meta-learner that jointly encodes time-domain and frequency-domain embeddings and performs per-class multi-prototype clustering in each view. Class evidence from the two domains is fused via a soft-OR (log-sum-exp) rule, yielding expressive and deployment-robust class representations under distribution shifts.
- We propose SGN to exploit raw statistical descriptors and infer both domain importance and prototype sensitivity. These data-driven priors coordinate the two views and stabilize meta-learning in unlabeled or previously unseen deployments.
- In the collaborative decision stage, each query uses SGN guidance to form a key and applies attention over the corresponding class-specific prototype sets, adaptively selecting and weighting the most relevant prototypes before producing the final logits. This query-aware aggregation improves cross-deployment generalization with limited supervision.

Extensive experiments on two real-world cross-deployment DFOS datasets show that the proposed framework consistently outperforms strong deep learning and meta-learning baselines, achieving more accurate and balanced activity recognition across diverse deployment configurations. By aligning the training objective with cross-deployment use, injecting sample-wise statistical priors to guide dual-domain fusion, and enabling instance level adaptation at decision time, these designs deliver stronger generalization with minimal data requirements.

## 2. Related Work

With the development of artificial intelligence (AI) technology, its application in distributed optical fiber vibration signal recognition is becoming increasingly widespread. Early research typically employed a paradigm combining feature extraction with traditional classifiers for event recognition. The features used included time-frequency domain statistical descriptors such as short-time Fourier transforms (Wu et al., 2022; Madsen et al., 2007), wavelet coefficients (Jia et al., 2019b), and Mel-frequency cepstral coefficients (MFCCs) (Wu et al., 2021). Common classification models include support vector machines (SVMs) (Qu et al., 2010; Xu et al., 2017), Gaussian mixture models (GMMs) (Tejedor et al., 2019, 2017), and hidden Markov models (HMMs) (Wu et al., 2019b). SVMs are often used for event classification in static scenarios, while GMMs/HMMs are used to model the statistical characteristics of time series signals and are suitable for handling the dynamic evolution of events. However, these generative models rely on complex parameter design and tuning processes and are generally less stable than discriminative models when sufficient training data is available. Additionally, some work has employed rule-driven heuristic methods, such as energy threshold detection, to achieve preliminary event recognition, but these methods struggle to generalize to complex patterns and diverse deployment scenarios.

To further model the temporal structure of signals, recurrent neural networks (RNNs) (Medsker et al., 2001) such as long short-term memory (LSTM) (Sherstinsky, 2020) networks have been introduced to capture the temporal dynamics of events. Compared with traditional static feature extraction methods based on sliding windows, RNN can continuously perceive contextual dependencies, thereby improving the recognition of persistent or periodic events. Furthermore, hybrid architectures such as CNN-RNN have been proposed to simultaneously capture local features and temporal dependencies, achieving good overall performance (Wang et al., 2016; Khaki et al., 2020). In recent years, the Transformer architecture has gradually demonstrated its powerful capabilities in signal modeling due to its global attention mechanism (Vaswani et al., 2017). Some work has introduced multi-branch or multi-scale Transformer architectures based on attention mechanisms to simultaneously account for different time scales and pattern complexity, achieving more refined event perception (Lim et al., 2021; Zhou et al., 2021). In some tasks, Transformers have even surpassed traditional CNN or RNN models, demonstrating their potential for modeling long-range dependencies and multimodal fusion.

Overall, deep learning methods have greatly improved the ability of distributed fiber optic systems to identify various vibration events, reduced feature engineering costs, and significantly lowered false alarm rates (He and Liu, 2021; Wu et al., 2019a, 2021). However, these methods still face two key challenges: First, they typically rely on a large number of labeled samples to support parameter training, but in actual deployments, data from different deployments and environmental conditions is often difficult to obtain. Second, when the distribution of the model differs between the training deployment and the test environment, per-

formance often degrades significantly, and the model lacks the ability to generalize across deployments. These limitations have prompted researchers to focus on learning mechanisms with greater adaptability and generalizability, such as meta-learning and domain generalization methods.

To address the domain shift challenge, Domain Generalization (DG) techniques have been proposed to learn domain-invariant representations from multiple source domains. Feature alignment methods, such as Deep CORAL (Sun and Saenko, 2016), align the second-order statistics of deep features between source and target distributions to reduce distributional discrepancies. Alternatively, robust optimization strategies like GroupDRO (Group Distributionally Robust Optimization) (Sagawa et al., 2019) explicitly optimize the model’s performance on the worst-case domain or group, preventing the model from relying on spurious correlations that do not hold across environments. While these DG methods significantly enhance robustness compared to standard empirical risk minimization, they typically aim for a static invariant model and lack the flexibility to actively adapt to specific target deployments using scarce support samples, which is the specific strength of meta-learning frameworks.

In distributed fiber optic sensing, domain shift is common. Changes in installation method, soil medium, or equipment can significantly affect signal characteristics, thus violating the training-testing identical distribution assumption. Meta-learning is a recently emerging strategy that aims to enable models to quickly adapt to new tasks or domains by training on a multi-task distribution.

Classic meta-learning algorithms such as MAML (Model-Agnostic Meta-Learning) and Prototypical Networks (ProtoNet) have achieved widespread success in fields such as computer vision (Finn et al., 2017; Snell et al., 2017). MAML simulates the fine-tuning process on multiple tasks to learn a parameter initialization that adapts to new tasks after a few gradient updates. ProtoNet is a metric learning method that uses the mean of each class’s samples in the embedding space as a prototype and classifies based on the nearest neighbor prototype. These methods have achieved significant performance improvements on standard few-shot learning benchmarks such as MiniImageNet, but they generally assume that the training and test tasks are distributed similarly.

Building on this foundation, researchers have also proposed a series of meta-learning methods with improvements across different dimensions. For example, R2D2 (Ridge Regression Differentiable Discriminator) (Bertinetto et al., 2018) introduces an analytical solver, enabling the model to perform stable and rapid feature fitting. ANIL (Almost No Inner Loop) (Raghu et al., 2019) emphasizes task specificity by focusing on the classifier layer, fine-tuning only top-level parameters while keeping the feature extractor fixed, reducing computational effort and overfitting risks. FEAT (Few-shot Embedding Adaptation with Transformer) (Ye et al., 2020) utilizes the Transformer module to perform context-aware adjustments to the support set embedding, improving the adaptability of prototype representation in small sample sizes. These methods expand the spectrum of meta-learning algorithms in terms of optimizer structure, parameter update paths, and representation flexibility, and demonstrate

differentiated advantages in few-shot and cross-domain tasks.

Research on meta-learning in the DFOS field is still in its early stages and faces numerous challenges. For example, tasks in each deployment scenario may have very few samples, and deployments vary significantly. Traditional meta-learning frameworks struggle to directly function in such non-stationary, multimodal, and high-noise scenarios. Furthermore, ProtoNet’s single prototype assumption is not applicable to event categories with significantly varying distributions; mechanisms such as multi-prototype representations or adaptive prototype aggregation become even more necessary in this context. Furthermore, because DFOS signals are long, high-dimensional sequences often accompanied by unstructured noise, meta-learning algorithms must also possess temporal modeling capabilities and robustness.

In summary, meta-learning approaches for domain generalization offer a potential path to addressing the generalization challenge of DFOS deployment by simulating distributional shifts during training, enabling models to adapt to new domains. However, existing methods such as MAML, ProtoNet, R2D2, ANIL, and FEAT still struggle with the multimodality, statistical bias, and uncertainty in prototype representation of DFOS data. This motivates us to design a more targeted architecture, namely the statistically guided dual-domain meta-learning framework proposed in this paper. By integrating statistical view guidance, dual-view multi-prototype aggregation, and query-aware decision-making mechanisms, this framework alleviates the adaptation bottlenecks of traditional meta-learning for DFOS tasks. The next section will detail the modeling details and innovative design of this framework.

### 3. Domain Generalization and Datasets

In a distributed fiber optic sensing (DFOS) system, the same action can produce significantly different signal responses under different deployment conditions. We obtained the action signal by phase demodulating the output signal of a Michelson interferometer system. Figure 1 shows a comparison of the climbing action signals under different deployment configurations. It can be seen that even the same action can exhibit drastically different signal characteristics under the influence of various environmental factors such as fiber installation location, contact materials, and installation methods. These factors lead to changes in coupling, spectral characteristics, and signal-to-noise ratio, resulting in domain shift. This makes it difficult to generalize models trained only in specific scenarios to other deployment environments.

To systematically study the impact of deployment changes on activity identification, we constructed two domain generalization datasets specifically for Distributed Fiber Optic Sensing (DFOS) systems: OSDG1 and OSDG2. Each dataset contains multiple deployment domains where the same set of activities is recorded under different fiber installation configurations. This design allows for controlled evaluation of cross-deployment generalization without introducing label inconsistencies. Due to differences in deployment across projects, signal lengths vary;

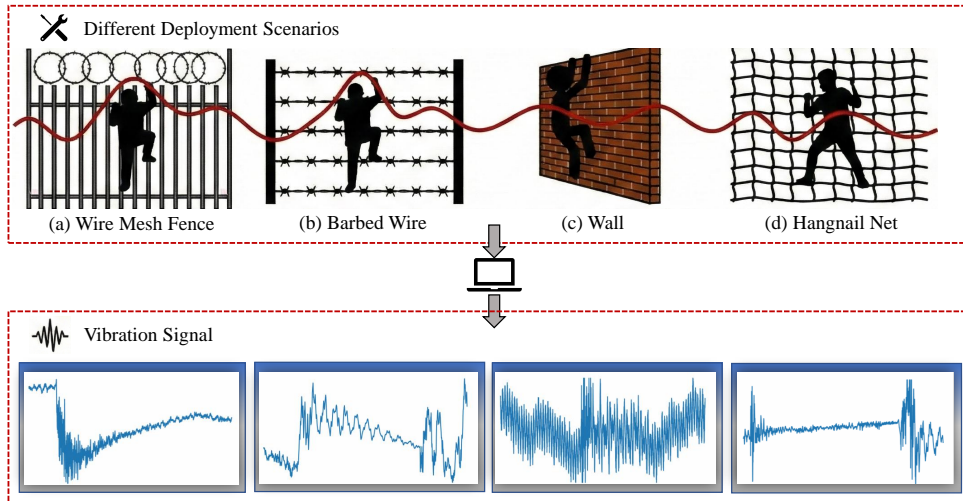


Figure 1: The figure shows the acquisition of climbing vibration signals under four different deployment methods. (a) is the acquisition under the wire mesh fence scenario, (b) is the acquisition under the barbed wire scenario, (c) is the acquisition under the wall scenario, and (d) is the acquisition under the hangnail net scenario. Due to differences in distance from the signal source, installation structure, or coupling conditions, the waveforms acquired under each deployment method show significant differences in amplitude, frequency distribution, and pulse characteristics.

these will be uniformly sampled to the same length during subsequent model preprocessing.

The OSDG1 dataset contains two deployment scenarios, representing typical perimeter security setups. In the first scenario, fiber optic cables are directly installed on traditional barbed wire. In the second scenario, fiber optic cables are fixed to a composite boundary structure consisting of a lower railing and an upper spiral barbed wire fence. Both scenarios recorded four types of events, including environmental context, human climbing activities, wind and rain, and the impact of human smash on the deployment environment. See Table 1 for details on the dataset size and distribution. Because this data was collected from a real-world project, acquiring signal data for specific actions was challenging, resulting in uneven data distribution and increasing the difficulty of model recognition.

Table 1: OSDG1 Dataset Quantity Distribution Table

Deployment method	Background	Climb	Rain	Smash
Barbed wire	70	125	80	104
Wire mesh fence	125	43	37	123

The OSDG2 dataset includes three different deployment conditions, covering a wider range of structural materials. See table 2 for dataset size details. Fiber optic cables were installed on Hangnail net, solid concrete walls, and Railing. Data for each deployment area comes from three action categories: environmental category, ladder climbing, and impact. All records were collected under consistent sensor parameters and sampling settings to ensure that regional differences are entirely attributable to the different deployment methods. The climbing category in OSDG2 differs from that in the OSDG1 dataset in that, in

most cases, people use ladders to climb safety facilities. The impact categories include human-made tools striking, rock impacts, and wildlife impacts. These factors also contribute to dividing this data into two separate datasets. Each dataset has a consistent label space across all deployment domains, enabling controlled cross-deployment evaluation, while the two datasets differ in class composition, deployment structures, and class imbalance, providing diverse levels of difficulty for DFOS domain generalization.

Table 2: OSDG2 Dataset Quantity Distribution Table

Deployment method	Background	Ladder climbing	Impact
Hangnail net	200	130	199
Wall	200	133	200
Railing	200	131	200

## 4. Method

### 4.1. Overall Framework Overview

Our meta-learning framework consists of three main components operating in concert: a dual-domain multi-prototype meta-learner, a statistical guidance network (SGN), and a collaborative decision module. As shown in Figure 2, the raw input is processed in parallel by time-domain and frequency-domain feature extractors, generating two sets of embeddings for the support and query samples, respectively. Furthermore, a global 26-dimensional statistical feature vector is extracted from each sample, which the SGN converts into a guidance signal and adjusts the weights. In a single training episode, the support embeddings in each domain are fed into the meta-learner to

## Main Process of the Model

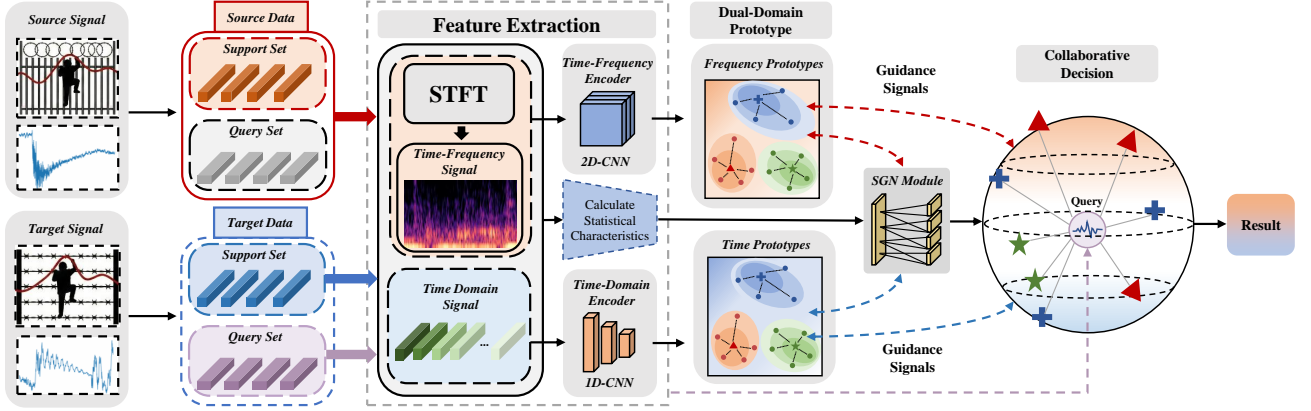


Figure 2: Overview of the proposed Dual-Domain Meta-Learning framework. The architecture first integrates temporal and spectral information via a Feature Extraction module, using parallel 1D-CNN and 2D-CNN. Based on these features, the system performs Dual-Domain Prototype Construction to capture intra-class diversity from the support set. In parallel, the SGN Module derives instance-specific guidance signals from the input’s statistical characteristics. This pipeline culminates in the Collaborative Decision module, which leverages the SGN guidance and a query-aware attention mechanism to adaptively aggregate prototypes for the final classification.

generate class prototypes and initial class predictions. These intermediate results from the dual domains are then coordinated by the collaborative decision module, which uses the guidance signal from the SGN to adaptively weight the contribution of each domain and perform query-aware prototype aggregation. The result is a final prediction for each query that reflects information from both the time and frequency domains. All components are jointly trained in an episodic manner, enabling the model to quickly adapt to new inference tasks by simply forwarding data through this fixed pipeline without the need for fine-tuning.

### 4.2. Dual-Domain Multi-Prototype Meta-Learner

To exploit complementary information, we extract features of fiber data in the time and frequency domains, respectively. Let  $x^{(t)}$  and  $x^{(f)}$  denote the original time-domain signal and its time-spectrogram of the sample, respectively.

In our implementation, the frequency-domain input  $x^{(f)}$  is constructed by Short-Time Fourier Transform (STFT). Given a raw 1-D signal segment sampled at  $f_s = 50$  kHz, we compute STFT using a Hann window with FFT size  $n_{\text{fft}} = 1024$  and hop length  $h = 512$  (i.e., 50% overlap). Let  $Z \in \mathbb{C}^{F \times T}$  denote the complex STFT; we take the magnitude spectrogram and apply logarithmic compression:  $x^{(f)} = \log(|Z| + \epsilon)$  with  $\epsilon = 10^{-8}$ . We then apply per-spectrogram standardization to zero mean and unit variance to stabilize the dynamic range. Finally, the spectrogram is padded/cropped to a fixed resolution of  $1 \times 513 \times 294$  (channel  $\times$  frequency bins  $\times$  time frames) before feeding into the frequency encoder.

We use two parallel feature extractors,  $f_t(\cdot)$  and  $f_f(\cdot)$ , where the 1DCNN extracts time-domain signal features and the 2DCNN extracts signal time-spectrogram features. They encode  $x^{(t)}$  and  $x^{(f)}$  into  $D$ -dimensional feature vectors,  $\mathbf{z}^{(t)} = f_t(x^{(t)}) \in \mathbb{R}^D$  and

$\mathbf{z}^{(f)} = f_f(x^{(f)}) \in \mathbb{R}^D$ . These embedding networks are designed to produce comparable feature representations for both domains (of dimension  $D = 128$  in our implementation). Given a labeled support set, we obtain a set of support embeddings in the time domain  $\mathbf{z}^{(t)}$  and the frequency domain  $\mathbf{z}^{(f)}$ . These two domains are handled independently by the same meta-learning logic, as described below.

We introduce an adaptive multi-prototype representation to capture the complex class distribution, rather than collapsing the support examples for each class into a single prototype as in standard prototypical networks. For each class  $c$ , we cluster the embeddings of the support examples  $\mathbf{z}_i^{(t)} : y_i = c$  and  $\mathbf{z}_i^{(f)} : y_i = c$ , generating  $K_c^{(t)}$  and  $K_c^{(f)}$  prototypes in the time and frequency domains, respectively. The number of prototypes  $K_c$  is dynamically determined based on the characteristics of the support set. This strategy is particularly useful when dealing with classes that exhibit diverse patterns, as it allows the model to represent the class with multiple prototype vectors, thereby enhancing its generalization ability.

For each class  $c$  in each domain  $d \in \{t, f\}$ , we determine the number of prototypes  $K_c^{(d)}$  in a data-driven manner. Let  $\mathcal{Z}_c^{(d)} = \{\mathbf{z}_i^{(d)} \mid y_i = c\}$  be the support embeddings of class  $c$  and  $N_c = |\mathcal{Z}_c^{(d)}|$ . We run  $K$ -means clustering on  $\mathcal{Z}_c^{(d)}$  with candidate  $K \in \{1, \dots, \min(K_{\max}, N_c)\}$  and obtain  $K$  centroids as prototypes. To select  $K_c^{(d)}$ , we compute the within-cluster sum of squares  $\text{WCSS}(K)$  and minimize a penalized criterion:

$$J(K) = \text{WCSS}(K) + \alpha \cdot K \cdot \log(\max(2, N_c)), \quad (1)$$

where  $\alpha$  controls the complexity penalty. The selected  $K_c^{(d)} = \arg \min_K J(K)$  balances intra-class multi-modality and over fragmentation. In our experiments, we set  $K_{\max} = 3$  and  $\alpha = 0.003$ .

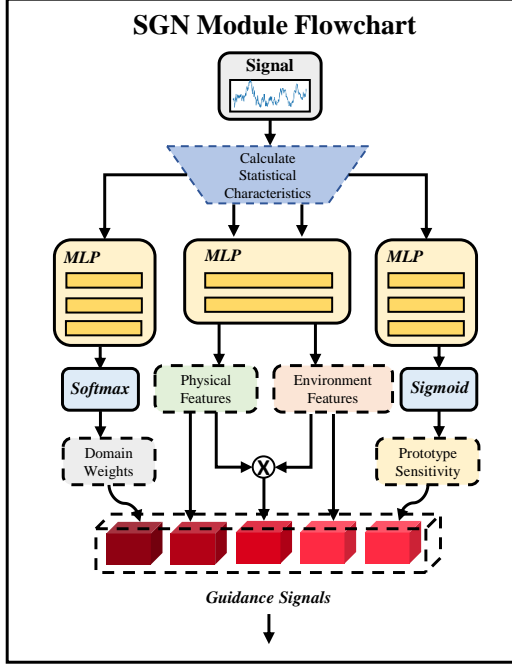


Figure 3: A schematic diagram of the Statistical Guidance Network (SGN) is shown. This module takes the statistical features of the input signal as input and obtains intermediate feature representations through a physical property analyzer and an environmental feature extractor composed of multi-layer MLPs, respectively. These two representations are then concatenated and mapped to the base guidance signal by a guidance signal generator. Furthermore, the statistical features are also input to a domain importance predictor and a prototype sensitivity predictor to estimate the sample’s dependence weights in the time and frequency domains, as well as its sensitivity to prototype aggregation, respectively. Finally, all guidance signals are output to downstream modules for dynamic adjustment.

After obtaining prototypes for each class in both domains, we compute the matching score between each query sample and the class prototype. Specifically, for each query sample  $\mathbf{z}_q$ , we use cosine similarity to measure the similarity between the query and each prototype. For domain  $d \in t, f$ , we calculate the similarity between the query embedding  $\mathbf{z}_q^{(d)}$  and each prototype  $\mathbf{c}_{c,k}^{(d)}$  of class  $c$ . The matching score of class  $c$  in domain  $d$  is calculated as follows:

$$\ell_c^{(d)}(q) = \log \sum_{k=1}^{K_c} \exp(\lambda \cdot \text{sim}(\mathbf{z}_q, \mathbf{c}_{c,k}^{(d)})). \quad (2)$$

where  $\text{sim}(\cdot, \cdot)$  is the cosine similarity between the query and prototype, and  $\lambda$  is a temperature scaling factor that controls the sharpness of the distribution. The result is a logit score  $\ell_c^{(d)}$  for each class  $c$  in both domains. The logits from both domains are then passed to the Collaborative Decision module for further fusion and decision-making.

### 4.3. Statistical Guidance Network (SGN)

The Statistical Guidance Network (SGN) plays a crucial role in our framework, providing context-aware guidance signals to regulate the learning process by analyzing global statistical features of the input data. Concretely, for each signal we extract

a 26-dimensional statistical feature vector  $\mathbf{s}$  composed of 16 time-domain features and 10 frequency-domain features. The definitions of these time-domain and frequency-domain features are summarized in Tables 3 and 4, respectively. These statistics capture global amplitude, energy and spectral characteristics that are not immediately apparent from the raw time-series or STFT representations, and are used to guide the meta-learner, provide domain-specific weights, and enhance the prototype matching process. The specific structure of the SGN is shown in Figure 3.

The SGN receives as input the 26-dimensional vector  $\mathbf{s}$  for each sample. This vector encodes various global properties of the signal, capturing information beyond the original time-domain or frequency-domain representations. The network consists of two sub-networks: one for extracting physical features and the other for extracting environmental context. Each sub-network processes  $\mathbf{s}$  and outputs latent vectors  $\mathbf{p}$  and  $\mathbf{e}$ , representing the physical and environmental characteristics of the signal, respectively.

These latent vectors are concatenated and fed into a guidance signal generation network, which generates a guidance vector  $\mathbf{g}$  that informs the meta-learner and decision module. The guidance vector is generated using the tanh activation function:

$$\mathbf{g} = \tanh(W_g[\mathbf{p}; \mathbf{e}] + \mathbf{b}_g). \quad (3)$$

where  $[\mathbf{p}; \mathbf{e}]$  is the concatenated vector of physical and environmental features, and  $W_g$  and  $\mathbf{b}_g$  are learnable weights and biases. The SGN also produces domain importance weights  $\alpha_t$  and  $\alpha_f$  for the time and frequency domains, respectively, which indicate the relative relevance of each domain. These weights are learned through a softmax function over the concatenated feature vector  $\mathbf{s}$ :

$$\alpha_t, \alpha_f = \text{softmax}(W_\alpha \mathbf{s} + b_\alpha). \quad (4)$$

In addition, the SGN generates a prototype sensitivity scalar  $\beta$ , which controls how strict or flexible the prototype matching should be. This scalar is learned to adapt based on the characteristics of the input sample. The outputs from the SGN—guidance vector  $\mathbf{g}$ , domain importance weights  $\alpha_t, \alpha_f$ , and prototype sensitivity  $\beta$ —are passed to the Collaborative Decision module, which uses them to adjust the predictions from the time and frequency domains.

### 4.4. Collaborative Decision with Query-Aware Attention

The Collaborative Decision module combines the predictions from both the time and frequency domains using query-aware attention. Its specific structure is shown in Figure 4. For each query sample, the module computes a query-specific key vector  $\mathbf{q}_c$ , which is a combination of the query’s guidance vector  $\mathbf{g}$  and its initial logits from the meta-learner. The query key vector  $\mathbf{q}_c$  is used to compute attention weights for each prototype in the time and frequency domains. Specifically, the attention weight for the  $k$ -th prototype of class  $c$  in domain  $d$  is calculated as:

$$a_{c,k}^{(d)} = \frac{\exp(\tau \text{sim}(\mathbf{q}_c, \mathbf{c}_{c,k}^{(d)}))}{\sum_{k=1}^{K_c^{(d)}} \exp(\tau \text{sim}(\mathbf{q}_c, \mathbf{c}_{c,k}^{(d)}))}. \quad (5)$$

Table 3: Time-domain statistical features.

Feature	Formula	Feature	Formula
Mean ( $S_1$ )	$\mu = \frac{1}{N} \sum_{n=1}^N x_n$	Std. dev. ( $S_2$ )	$\sigma = \sqrt{\frac{1}{N} \sum_{n=1}^N (x_n - \mu)^2}$
Variance ( $S_3$ )	$\sigma^2 = \frac{1}{N} \sum_{n=1}^N (x_n - \mu)^2$	Maximum ( $S_4$ )	$\max_n x_n$
Minimum ( $S_5$ )	$\min_n x_n$	Peak-to-peak ( $S_6$ )	$\max_n x_n - \min_n x_n$
RMS ( $S_7$ )	$\sqrt{\frac{1}{N} \sum_{n=1}^N x_n^2}$	Skewness ( $S_8$ )	$\text{skew}(x) = \frac{1}{N} \sum_{n=1}^N \left(\frac{x_n - \mu}{\sigma}\right)^3$
Kurtosis ( $S_9$ )	$\text{kurt}(x) = \frac{1}{N} \sum_{n=1}^N \left(\frac{x_n - \mu}{\sigma}\right)^4$	Mean abs. value ( $S_{10}$ )	$\frac{1}{N} \sum_{n=1}^N  x_n $
Median ( $S_{11}$ )	$\text{median}(\{x_n\})$	IQR ( $S_{12}$ )	$Q_3 - Q_1$
Signal energy ( $S_{13}$ )	$E = \sum_{n=1}^N x_n^2$	Average energy ( $S_{14}$ )	$\frac{E}{N}$
Zero-crossing rate ( $S_{15}$ )	$\text{ZCR} = \frac{N_{zc}}{N}$	Peak density ( $S_{16}$ )	$\text{PD} = \frac{N_{peaks}}{N}$

Table 4: Frequency-domain statistical features.

Feature	Formula	Feature	Formula
Spec. mean mag. ( $S_{17}$ )	$\frac{1}{K} \sum_{k=1}^K  X(f_k) $	Spec. std. ( $S_{18}$ )	$\sqrt{\frac{1}{K} \sum_{k=1}^K ( X(f_k)  - \bar{A})^2}$
Spec. max mag. ( $S_{19}$ )	$\max_k  X(f_k) $	Spec. min mag. ( $S_{20}$ )	$\min_k  X(f_k) $
Spectral centroid ( $S_{21}$ )	$f_c = \frac{\sum_k f_k  X(f_k) }{\sum_k  X(f_k) }$	Spectral bandwidth ( $S_{22}$ )	$\sqrt{\frac{\sum_k (f_k - f_c)^2  X(f_k) }{\sum_k  X(f_k) }}$
Spectral roll-off ( $S_{23}$ )	$\sum_{f_k \leq f_r}  X(f_k) ^2 \geq 0.95 \sum_k  X(f_k) ^2$	Spectral flatness ( $S_{24}$ )	$\frac{\exp(\frac{1}{K} \sum_{k=1}^K \ln  X(f_k) )}{\frac{1}{K} \sum_{k=1}^K  X(f_k) }$
Dominant frequency ( $S_{25}$ )	$f_{\text{dom}} = f_{k^*}, k^* = \arg \max_k  X(f_k) $	Spectral entropy ( $S_{26}$ )	$H = -\sum_k p_k \log_2 p_k, p_k = \frac{ X(f_k) }{\sum_j  X(f_j) }$

Where  $\tau$  is a learned temperature parameter. The attention weights  $a_{c,k}^{(d)}$  reflect how relevant each prototype is to the current query, with higher weights corresponding to prototypes that are more similar to the query. These attention weights are then used to aggregate the prototypes into a representative prototype for class  $c$  in domain  $d$ :

$$\mathbf{r}_c^{(d)} = \sum_{k=1}^{K_c^{(d)}} a_{c,k}^{(d)} \mathbf{c}_{c,k}^{(d)}. \quad (6)$$

These representative prototypes  $\mathbf{r}_c^{(t)}$  and  $\mathbf{r}_c^{(f)}$  are then passed through a cross-domain relation network, which models the relationship between the two domains. The relation vector  $\mathbf{v}_c$  captures the consistency between the time-domain and frequency-domain representations for class  $c$ :

$$\mathbf{v}_c = f_{\text{relation}}([\mathbf{r}_c^{(t)}; \mathbf{r}_c^{(f)}]). \quad (7)$$

The relation vector  $\mathbf{v}_c$  is passed through a decision network that combines it with the domain importance weights  $\alpha_t$  and  $\alpha_f$  to produce the final logit for class  $c$ :

$$\ell_c^{\text{final}} = \alpha_t \ell_c^{(t)} + \alpha_f \ell_c^{(f)} + h(\mathbf{v}_c, \alpha_t, \alpha_f, \kappa_t, \kappa_f). \quad (8)$$

Where  $h(\cdot)$  is a fully-connected decision network that integrates the information from both domains. This final logit is used to make the prediction for the query sample, completing the decision process.

## 5. Experiments

All experiments were implemented using PyTorch on an NVIDIA vGPU-32GB platform. We evaluate our framework on

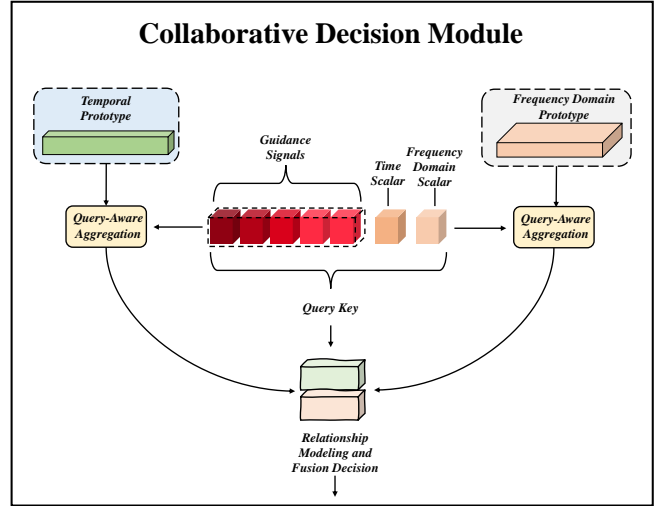


Figure 4: A schematic diagram of the Collaborative Decision module. The time-domain and frequency-domain prototypes are processed through two aggregation branches based on queries. The query consists of a guiding signal and two scalars in the time and frequency domains, which are used to modulate the two branches. The aggregation results from both paths are fed into the relation modeling unit and fused to obtain the final decision.

Table 5: Comparison of Traditional, Deep Learning, and Domain Generalization Baselines on OSDG1 and OSDG2 (in %).

Model	OSDG1 (%)				OSDG2 (%)			
	Accuracy	Precision	Recall	F1	Accuracy	Precision	Recall	F1
Xgboost(Chen and Guestrin, 2016)	26.58 ± 16.89	19.70 ± 10.87	33.52 ± 6.60	20.76 ± 10.42	56.57 ± 47.65	68.51 ± 37.90	57.93 ± 48.07	57.72 ± 45.78
SVM(Qu et al., 2010)	26.02 ± 13.95	21.45 ± 19.11	34.34 ± 3.12	23.62 ± 15.58	53.74 ± 47.00	58.96 ± 48.43	55.30 ± 47.73	53.25 ± 46.45
KNN(Jia et al., 2019a)	37.48 ± 13.83	42.54 ± 11.15	34.92 ± 10.38	29.68 ± 9.92	60.26 ± 11.89	64.50 ± 17.84	63.64 ± 9.45	56.52 ± 13.83
1DCNN(Wu et al., 2019a)	34.64 ± 13.53	21.56 ± 1.19	35.20 ± 6.59	22.64 ± 6.77	57.38 ± 16.79	41.21 ± 24.31	51.77 ± 15.90	44.09 ± 22.38
2DCNN(Xu et al., 2018)	42.15 ± 11.10	50.94 ± 2.13	45.42 ± 6.12	38.32 ± 8.07	57.31 ± 15.98	68.52 ± 19.53	58.39 ± 20.19	49.44 ± 24.08
LSTM(Sherstinsky, 2020)	23.19 ± 11.24	15.47 ± 1.65	30.57 ± 0.52	18.33 ± 1.03	67.72 ± 8.27	57.36 ± 15.68	62.69 ± 9.92	57.26 ± 12.27
Transformer(Vaswani et al., 2017)	22.03 ± 3.55	22.37 ± 3.39	27.93 ± 0.81	21.41 ± 3.95	68.69 ± 15.87	70.67 ± 14.38	67.41 ± 13.47	65.92 ± 15.19
GroupDRO(Sagawa et al., 2019)	57.82 ± 16.10	58.87 ± 16.49	52.90 ± 3.12	48.22 ± 10.46	71.72 ± 14.23	75.13 ± 22.09	74.78 ± 12.36	68.15 ± 18.23
Coral(Sun and Saenko, 2016)	52.21 ± 11.53	57.69 ± 6.97	49.81 ± 3.30	44.32 ± 13.16	70.10 ± 12.25	85.65 ± 3.69	71.07 ± 6.89	64.43 ± 12.67

Table 6: Few-Shot Accuracy Comparison on OSDG1 and OSDG2 Datasets (in %).

Model	OSDG1 (Shots, %)				OSDG2 (Shots, %)			
	1-shot	3-shot	5-shot	10-shot	1-shot	3-shot	5-shot	10-shot
ProtoNet(Snell et al., 2017)	32.71 ± 4.93	31.51 ± 5.57	31.55 ± 5.84	30.80 ± 6.88	65.09 ± 11.65	66.65 ± 11.55	66.49 ± 10.77	66.67 ± 10.22
MAML(Finn et al., 2017)	38.89 ± 11.39	39.76 ± 12.63	39.78 ± 12.13	39.66 ± 11.87	62.56 ± 15.59	63.86 ± 13.69	64.64 ± 13.73	64.87 ± 13.86
ANIL(Raghu et al., 2019)	30.95 ± 7.54	35.15 ± 11.99	35.34 ± 11.87	36.31 ± 13.42	58.87 ± 21.49	62.61 ± 18.63	63.31 ± 19.08	63.67 ± 20.21
R2D2(Bertinetto et al., 2018)	41.34 ± 8.81	40.49 ± 8.09	40.24 ± 8.04	40.18 ± 7.88	54.26 ± 20.19	63.34 ± 22.98	64.00 ± 23.91	64.25 ± 24.74
FEAT(Ye et al., 2020)	47.29 ± 6.00	49.11 ± 9.82	49.53 ± 9.07	48.80 ± 9.69	53.32 ± 5.80	57.43 ± 11.49	57.74 ± 12.90	58.35 ± 14.69
<b>DUPLE (Ours)</b>	58.73 ± 2.39	62.76 ± 2.65	63.07 ± 3.56	63.66 ± 3.23	68.17 ± 15.34	77.06 ± 18.98	77.45 ± 20.35	77.20 ± 22.73

two real-world cross-deployment datasets, OSDG1 and OSDG2, utilizing a rigorous Leave-One-Deployment-Out (LODO) cross-validation protocol. Specifically, we iteratively designate one deployment as the unseen target domain (TEST) while training on the remaining deployments (TRAIN), reporting the mean Accuracy, Precision, Recall, and F1 Score across all folds (2 folds for OSDG1, 3 folds for OSDG2). This protocol strictly simulates real-world deployment shifts, where the high variance in our reported results reflects the varying degrees of domain discrepancy across different physical environments.

For meta-learning evaluations, we adopt a standard episodic protocol ( $N$ -way  $K$ -shot  $Q$ -query). We define  $N=4$  for OSDG1 and  $N=3$  for OSDG2, with a fixed query size of  $Q=12$  to ensure class balance. The main comparative experiments are conducted under a 5-shot setting ( $K=5$ ), evaluated over 1,000 randomly sampled episodes to ensure statistical reliability. Consistent with the domain generalization setting, no target domain labels are utilized for model adaptation during inference.

### 5.1. Comparative Experiment

To rigorously evaluate the efficacy of the proposed DUPLE framework, we conducted comprehensive comparative experiments on the OSDG1 and OSDG2 datasets. We benchmarked our method against a diverse set of baselines, ranging from traditional machine learning algorithms to standard deep learning models, domain generalization (DG) techniques, and state-of-the-art meta-learning frameworks.

Table 5 summarizes the performance of non-meta-learning approaches. First, traditional machine learning methods such as XGBoost and SVM exhibit limited efficacy in these cross-deployment scenarios. On the OSDG1 dataset, their accuracies remain below 30%, indicating that manual feature engineering is insufficient to capture invariant patterns amidst severe domain shifts.

Table 7: Per-deployment macro-F1 breakdown under LODO evaluation. Meta-learning models are evaluated at 5-shot setting.

Model	OSDG1 (Deployments, %)		OSDG2 (Deployments, %)		
	Wire Mesh Fence	Barbed Wire	Hangnail Net	Railing	Wall
GroupDRO	55.62	40.83	89.05	59.84	55.56
ProtoNet	22.73	34.44	70.98	69.86	54.77
FEAT	39.52	52.68	46.37	67.15	37.98
<b>DUPLE (Ours)</b>	60.48	65.71	95.02	81.80	51.81

Second, standard deep learning models demonstrate significant performance variability driven by architecture bias. On OSDG1, the 2DCNN utilizes Time-Frequency (STFT) representations to achieve 42.15% accuracy, which is notably superior to raw-signal-based models like the 1DCNN at 34.64% and the Transformer at only 22.03%. Conversely, the performance trend on OSDG2 shifts dramatically to favor sequence-based models, where the Transformer and LSTM models achieve leading accuracy rates of 68.69% and 67.72%, respectively, significantly outperforming convolutional architectures. This inconsistency highlights that standard supervised learning architectures often overfit to domain-specific feature modalities.

Most notably, the Domain Generalization (DG) baselines, GroupDRO and Deep CORAL, demonstrate superior robustness compared to standard Empirical Risk Minimization (ERM) models. To ensure a fair comparison, we implemented these DG algorithms using the same 2DCNN backbone as the standard baseline. By explicitly optimizing for worst-case groups or aligning feature distributions, these methods establish a strong performance baseline. On the challenging OSDG1 dataset, GroupDRO reaches an accuracy of 57.82%, surpassing the standard 2DCNN by a margin of over 15%. Similarly, on OSDG2, GroupDRO and Coral maintain the lead with accuracies of 71.72% and 70.10%, respectively. However, despite their higher average accuracy,

Table 8: Few-Shot F1 Comparison on OSDG1 and OSDG2 Datasets (in %).

Model	OSDG1 (Shots, %)				OSDG2 (Shots, %)			
	1-shot	3-shot	5-shot	10-shot	1-shot	3-shot	5-shot	10-shot
ProtoNet(Snell et al., 2017)	26.20 ± 1.40	24.30 ± 2.08	24.28 ± 2.19	23.54 ± 3.08	64.14 ± 9.90	65.56 ± 9.83	65.20 ± 9.05	65.30 ± 8.52
MAML(Finn et al., 2017)	35.83 ± 10.87	35.09 ± 12.51	34.65 ± 12.43	34.27 ± 12.12	61.55 ± 15.00	62.33 ± 13.11	63.05 ± 13.21	63.12 ± 13.49
ANIL(Raghu et al., 2019)	30.15 ± 6.99	33.42 ± 10.34	33.43 ± 10.19	33.88 ± 11.25	57.92 ± 21.77	60.12 ± 21.38	60.23 ± 22.78	60.18 ± 24.63
R2D2(Bertinetto et al., 2018)	38.20 ± 16.70	37.21 ± 16.03	36.87 ± 16.00	36.86 ± 15.85	54.91 ± 19.59	63.67 ± 22.69	64.10 ± 23.90	64.02 ± 25.15
FEAT(Ye et al., 2020)	44.28 ± 7.75	45.43 ± 10.92	46.10 ± 9.31	44.30 ± 9.81	48.71 ± 7.62	51.25 ± 13.80	50.50 ± 15.02	49.97 ± 16.65
<b>DUPLE (Ours)</b>	58.58 ± 2.60	62.70 ± 2.98	63.09 ± 3.69	63.92 ± 3.19	66.43 ± 18.26	75.36 ± 21.59	76.21 ± 22.14	76.02 ± 24.42

Table 9: Statistical significance (Welch’s  $t$ -test) against the best meta-learning baseline over 1,000 episodes.

Dataset	Best Baseline †	DUPLE (Ours)	$p$ -value	Significant?
OSDG1	49.53 ± 9.07 (FEAT)	63.07 ± 3.56	$< 10^{-4}$	<b>Yes</b>
OSDG2	66.49 ± 10.77 (ProtoNet)	77.45 ± 20.35	$< 10^{-4}$	<b>Yes</b>

† The best baseline varies by dataset: FEAT for OSDG1, ProtoNet for OSDG2.

these DG methods exhibit high variance, exemplified by the standard deviation of 16.10% observed for GroupDRO on OSDG1. This instability underscores a critical limitation: purely invariant representation learning without test-time adaptation is often insufficient to guarantee consistent performance across highly diverse optical fiber deployment environments.

Tables 6 and 8 present the few-shot classification results. In general, meta-learning baselines exhibit improved generalization capabilities compared to standard deep models, particularly in low-data regimes. On OSDG1, FEAT emerges as the strongest baseline with a 5-shot accuracy of 49.53%. In contrast, standard metric-based methods such as ProtoNet perform suboptimally, yielding only 31.55%. This underperformance suggests that a unimodal single-prototype representation is inadequate for modeling the complex, multi-modal distribution of fiber signals in this highly shifted scenario. On OSDG2, ProtoNet demonstrates robust performance by achieving 66.49% accuracy, which outperforms more complex architectures like R2D2 and ANIL that reach 64.00% and 63.31% respectively. This indicates that for certain deployment configurations where the domain gap is moderate, the feature space is sufficiently discriminative for Euclidean-distance-based metrics.

The proposed DUPLE framework consistently establishes a new state-of-the-art across both datasets and all shot settings, effectively mitigating the performance gaps observed in baseline methods. Specifically, on the challenging OSDG1 dataset (5-shot), DUPLE achieves an accuracy of 63.07%, surpassing the best-performing meta-learning baseline, FEAT, by a substantial margin of over 13.5%. This significant improvement validates the efficacy of our dual-domain fusion strategy in extracting domain-invariant representations under conditions where single-domain baselines struggle. Similarly, in the OSDG2 scenario, our method attains an accuracy of 77.45%. This performance not only surpasses the strongest meta-learning baseline, ProtoNet, by approximately 11%, but also outperforms the leading domain generalization baseline, GroupDRO (71.72%), by a clear margin of 5.73%.

Notably, we report results as mean ± standard deviation over

LODO folds (OSDG1: 2 deployments; OSDG2: 3 deployments), where the standard deviation reflects cross-deployment heterogeneity rather than random instability. In particular, OSDG2 exhibits larger variability because different held-out deployments pose substantially different difficulty levels. As evidenced by the per-deployment macro-F1 breakdown in Table 7, DUPLE achieves 95.02% on Hangnail net and 81.80% on Railing, but drops to 51.81% on Wall, indicating that Wall constitutes a significantly more challenging deployment scenario. Similar cross-deployment fluctuations are observed for ProtoNet and GroupDRO, confirming that the higher standard deviations primarily arise from real deployment shifts captured by the LODO protocol. Overall, DUPLE’s superior mean performance amid such heterogeneity confirms its robustness under both moderate and severe domain shifts.

To verify that these performance gains are statistically reliable rather than artifacts of random episodic sampling, we conducted Welch’s  $t$ -tests over 1,000 testing episodes. As detailed in Table 9, we compared DUPLE against the strongest baseline for each dataset. The resulting  $p$ -values are significantly below  $10^{-4}$  in both scenarios, providing strong statistical evidence that DUPLE yields a significant performance improvement over existing state-of-the-art methods.

In conclusion, DUPLE not only surpasses conventional deep models and DG algorithms in generalization capability but also addresses the representational limitations of existing meta-learners. By effectively fusing dual-domain features with adaptive prototype aggregation, it achieves the highest Accuracy and F1 Scores across heterogeneous deployment environments.

## 5.2. Ablation Experiment and Mechanism Analysis

### 5.2.1. Ablation Experiment

To systematically dissect the contribution of each component within the DUPLE framework, we conducted ablation studies using the same rigorous Leave-One-Deployment-Out protocol as the main experiments. We evaluated three core modules: the Dual-Domain Multi-Prototype Learner (FPM), the Statistical Guidance Network (SGN), and the Query-Aware Collaborative

Decision Making (CDM). The results are summarized in Table 10.

We conducted systematic ablation experiments to isolate the contributions of the FPM, SGN, and CDM modules, yielding consistent improvements across both datasets. First, the Dual-Domain Multi-Prototype Learner (FPM) acts as the primary performance driver, effectively characterizing intra-class diversity across deployments; it alone boosts accuracy from the baseline’s 49.86% to 57.79% on OSDG1. Building on this foundation, the Statistically Guided Network (SGN) and Collaborative Decision Making (CDM) modules provide complementary gains. SGN utilizes sample statistics to regularize domain importance, while CDM dynamically refines prototype weights based on the query. Contrary to unguided aggregation, the inclusion of either module yields distinct performance boosts, confirming that both statistical priors and query-aware attention are essential for robust feature alignment under domain shifts.

Overall, the integration of all three modules in the complete DUPLE framework delivers remarkable results. The full model achieves double-digit accuracy improvements compared to the naive baseline, advancing from 49.86% to 63.09% on OSDG1 and from 60.03% to 77.45% on OSDG2. Notably, while the standard deviation on OSDG2 remains high ( $\pm 20.35\%$ ) due to the intrinsic difficulty variances captured by our Leave-One-Deployment-Out protocol, the mean performance consistently surpasses all ablated variants. By combining dual-domain prototypes with statistical and query-based guidance, our approach significantly mitigates the domain shift problem, offering a stable and accurate solution for diverse deployment environments.

### 5.2.2. Robustness to Data Scarcity

In practical engineering deployments, collecting labeled data for new scenarios is often costly and labor-intensive. To rigorously assess the efficacy of DUPLE in low-data regimes, we conducted experiments with support set sizes ranging from  $K = 1$  to 10 on both OSDG1 and OSDG2 datasets. Beyond Accuracy, we also analyzed Precision and F1-Score to assess the trade-off between false alarms and missed detections. Figure 5 presents the results.

On the challenging OSDG1 dataset, DUPLE demonstrates a commanding advantage over all baselines. As illustrated in Figures 5(a) and (c), our method maintains a significant lead in both Accuracy and F1 Score across all  $K$  values. Notably, under extreme single-sample conditions ( $K = 1$ ), DUPLE achieves an F1 Score exceeding 58%, whereas the strongest baseline (FEAT) hovers around 44%, and standard metric-based methods like ProtoNet drop below 27%. This substantial gap confirms that the SGN module successfully prevents model collapse even with minimal supervision. Furthermore, as depicted in Figure 5(b), DUPLE achieves the highest Precision across the board, indicating its ability to learn robust discriminative features without succumbing to the low-precision pitfalls seen in baseline methods.

For the OSDG2 dataset, the results reveal DUPLE’s superior learning potential. As shown in Figures 5(d) and (f), while DUPLE starts with a moderate lead at  $K = 1$ , it exhibits a rapid performance gain as the support set size increases to  $K = 3$ ,

establishing a clear dominance thereafter. Crucially, unlike many baselines that trade Recall for Precision, DUPLE achieves the highest performance in both metrics simultaneously. In Figure 5(e), DUPLE’s Precision climbs from 69% at 1-shot to over 84% at 10-shot, significantly outperforming the next best method. This overall advantage is reflected in the F1 score, as shown in Figure 5(f), where DUPLE’s F1 score is more than 10% higher than that of the best baseline model, ProtoNet. Since the F1 Score represents the harmonic mean of Precision and Recall, DUPLE’s top-tier performance on this metric indicates that it provides the most robust solution for practical security monitoring, achieving an optimal balance between false positives and false negatives.

### 5.2.3. Feature Space Visualization

To qualitatively assess the discriminative structure of the learned representations, we employ t-SNE to project the high-dimensional query embeddings into a two-dimensional space for visualization. Under the rigorous Leave-One-Deployment-Out (LODO) protocol, the feature geometry may vary across folds due to deployment-specific signal characteristics. To provide a representative and reproducible view without cherry-picking, we report the embeddings from the most challenging deployment fold for each dataset, identified by the lowest silhouette score in the learned embedding space. Accordingly, the visualizations correspond to the Barbed wire deployment for OSDG1 and the Railing deployment for OSDG2 (Fig. 6).

In the more challenging OSDG1 setting, Fig. 6(a) reveals a heterogeneous embedding structure under strong deployment-induced variations. The Smash samples form a compact and well-separated cluster, whereas Climb exhibits pronounced fragmentation into multiple scattered sub-clusters, with noticeable mixing with Background and Rain. This pattern reflects substantial intra-class variability and deployment-specific distribution shifts, which is consistent with the more difficult quantitative results reported in Table 5. Importantly, despite the fragmented structure, the embeddings do not collapse into a single indistinguishable region, indicating that DUPLE still preserves meaningful class-related structures under this challenging deployment.

In contrast, Fig. 6(b) shows that OSDG2 (Railing) yields a more structured organization of the embedding space, with clearer separation among Background, Climb, and Impact and reduced inter-class mixing compared with OSDG1. This observation aligns with the stronger performance of DUPLE on OSDG2, suggesting that the proposed dual-domain and prototype-based metric learning can produce more consistent class-wise clustering under certain deployment conditions.

### 5.3. Computational Efficiency Analysis

To assess the deployment feasibility of the proposed method in real-time monitoring systems, we benchmarked the model complexity (Parameters), computational cost (FLOPs), and inference latency against representative baselines. All evaluations were conducted on a single NVIDIA VGPU-32GB using a batch size of 1 to simulate the sequential data processing typical of edge computing environments. The standardized input length was set to 150,000 sampling points.

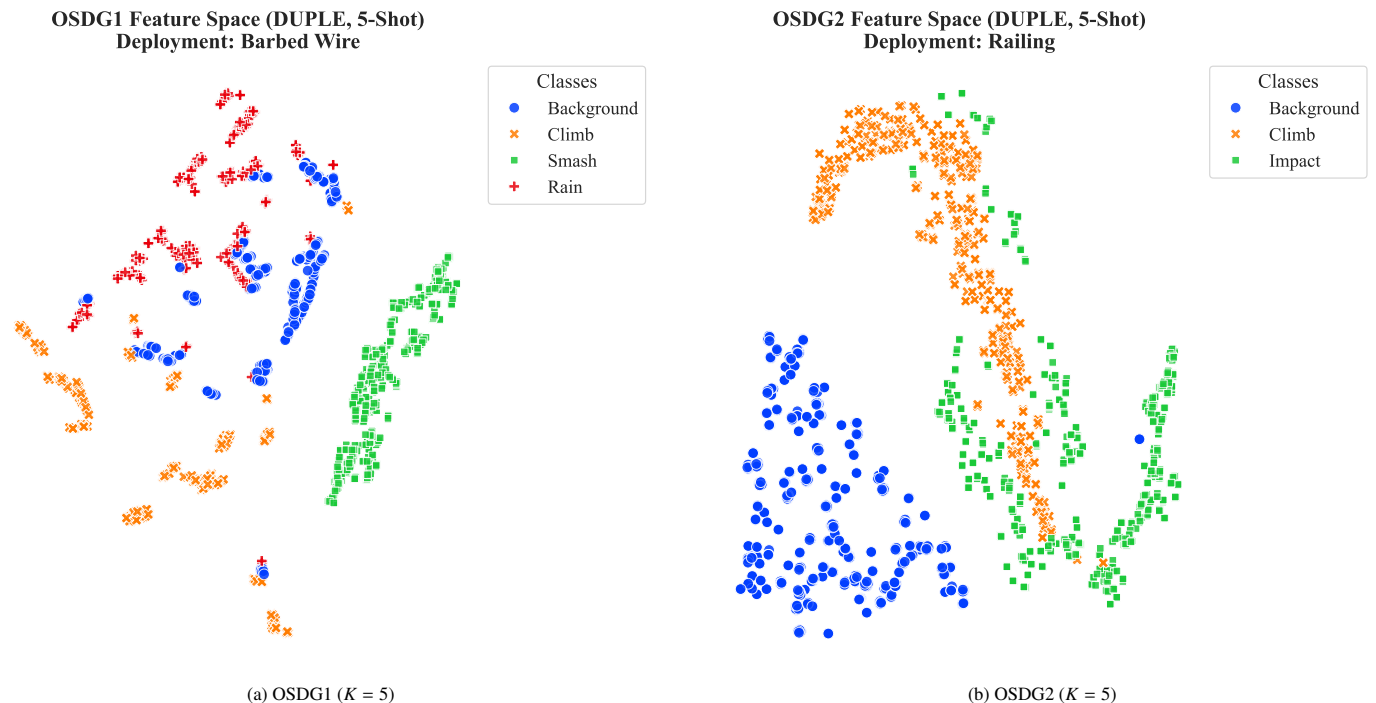
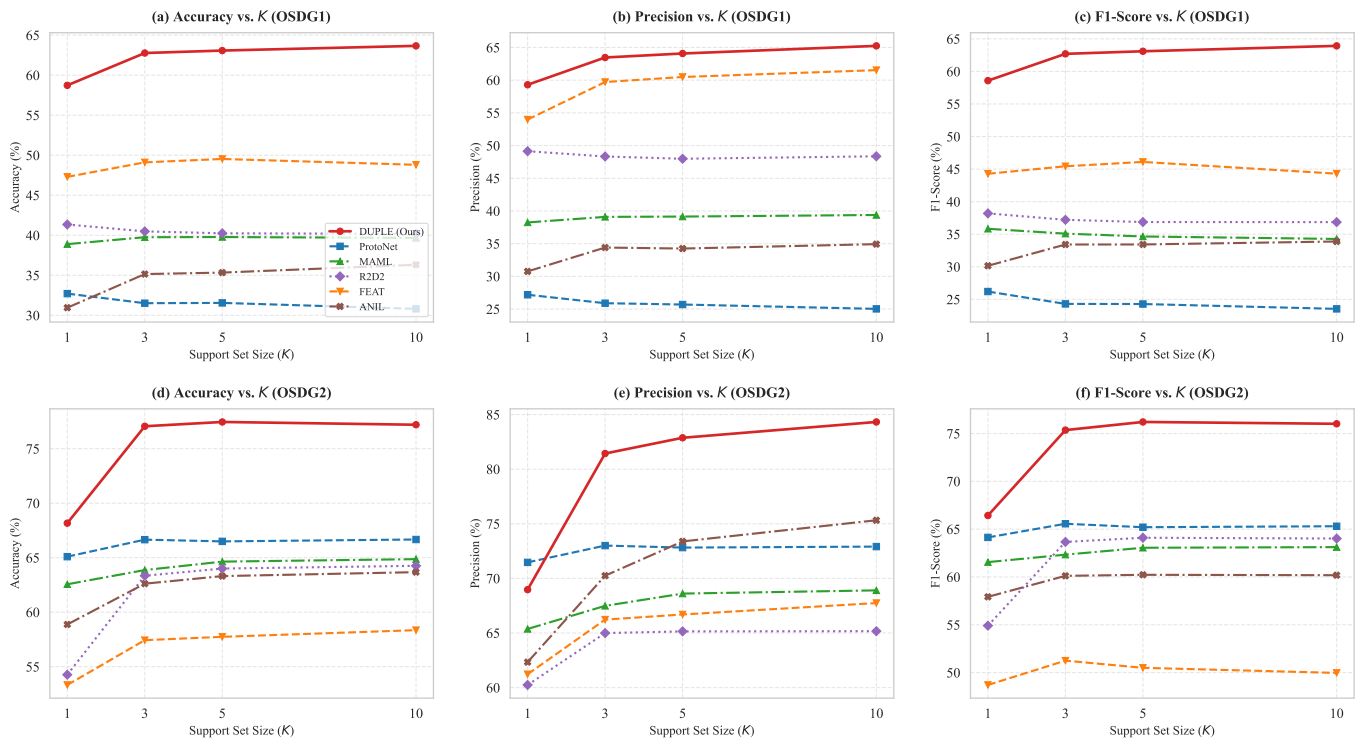


Figure 6: t-SNE visualization of the feature embeddings learned by DUPLÉ (5-shot) on representative held-out deployments. (a) **OSDG1(Barbed wire)**: Smash forms a compact and well-separated cluster, whereas Climb is highly fragmented into multiple scattered sub-clusters and shows noticeable mixing with Background and Rain. This pattern reflects strong deployment-induced variability and helps explain the more challenging performance on OSDG1. (b) **OSDG2(Railing)**: The embeddings exhibit clearer class separation among Background, Climb, and Impact, with substantially reduced inter-class mixing compared with OSDG1, consistent with the stronger quantitative results on OSDG2.

Table 10: Ablation Study of DUPLE Modules (5-Shot). Results in %.

Module			OSDG1 (%)				OSDG2 (%)			
FPM	SGN	CDM	Accuracy	Precision	Recall	F1	Accuracy	Precision	Recall	F1
-	-	-	49.86 ± 3.17	50.22 ± 2.85	49.86 ± 3.17	49.28 ± 3.86	60.03 ± 20.47	58.98 ± 22.07	60.03 ± 20.47	57.35 ± 22.15
✓	-	-	57.79 ± 2.80	59.09 ± 4.01	57.79 ± 2.80	56.20 ± 1.91	66.62 ± 24.60	70.81 ± 21.93	66.62 ± 24.60	64.89 ± 26.18
✓	✓	-	61.07 ± 0.93	62.33 ± 2.47	61.07 ± 0.93	59.88 ± 0.30	66.70 ± 24.55	70.94 ± 21.63	66.70 ± 24.55	64.98 ± 26.14
✓	-	✓	60.14 ± 0.75	60.85 ± 0.09	60.14 ± 0.75	59.20 ± 1.75	67.53 ± 23.70	71.46 ± 20.93	67.53 ± 23.70	65.67 ± 25.45
✓	✓	✓	63.07 ± 3.56	64.08 ± 4.35	63.07 ± 3.56	63.92 ± 3.19	77.45 ± 20.35	82.87 ± 11.94	77.45 ± 20.35	76.21 ± 22.14

Table 11: Comparison of computational efficiency. The metrics were measured on a single NVIDIA vGPU-32GB with batch size = 1, using standardized input signals of 150,000 sampling points (~3 s at 50 kHz). Time (ms) reports the model inference latency excluding STFT preprocessing and data I/O.

Model	Params (M)	FLOPs (G)	Time (ms)	FPS
1D-CNN	0.01	0.11	0.13	7690.11
2D-CNN	0.04	0.74	0.15	6840.92
Transformer	1.19	0.31	0.61	1634.76
ProtoNet	2.44	1.65	1.46	685.71
<b>DUPLE (Ours)</b>	2.48	3.30	6.12	163.42

Table 11 summarizes the efficiency metrics. Traditional deep learning models, especially 1D-CNN and 2D-CNN, have the lowest computational overhead, with inference times below 0.2 milliseconds. However, their limited parameter capacities of 0.01 M and 0.04 M, respectively, restrict feature representation and lead to poor generalization performance. While Transformer models maintain a moderate inference speed, their accuracy is lower compared to meta-learning methods, indicating that standard attention mechanisms alone are insufficient for this specific cross-domain few-shot task.

Compared to the ProtoNet baseline model, our proposed DUPLE framework introduces higher computational load and latency, at 3.30 G FLOPs and 6.12 ms, respectively. This increase is attributed to the parallel processing architecture of the dual-domain branches and the additional computation required for instance-level reweighting by the SGN module. Although DUPLE is slower than lightweight baselines, it still satisfies real-time DFOS monitoring with a large margin (6.12 ms per ~3 s window). Nevertheless, DUPLE achieves an inference speed of approximately 163 FPS. Considering that typical distributed fiber optic sensing systems require alarm response frequencies of 20 Hz to 50 Hz, DUPLE’s processing speed is sufficient to support real-time operation. Therefore, the proposed method achieves a practical trade-off, significantly improving accuracy without violating latency constraints in industrial deployments.

#### 5.4. Comparison Experiments by Category

While overall accuracy provides a general measure of performance, it can obscure critical failures in specific classes, particularly under the imbalance induced by domain shifts. Therefore, we conduct a fine-grained analysis to determine whether models maintain reliable detection capabilities across all intrusion types or merely overfit to majority classes.

Analysis of OSDG1. As detailed in Table 12, standard deep learning baselines on OSDG1 suffer from catastrophic mode collapse. Notably, the 1DCNN failed to identify a single sample from the Background or Climb classes, yielding 0.00% accuracy in both cases, likely due to overfitting on the Smash class where it reached 76.87%. Even robust Domain Generalization (DG) methods exhibited significant instability; while GroupDRO performed well on Rain and Smash, it struggled severely with the Background class, achieving an accuracy of only 18.60%. This indicates that optimizing for worst-case groups does not fully resolve feature ambiguity in this domain.

Meta-learning baselines also demonstrated severe class selectivity. ProtoNet performed adequately on Background samples but its detection rate for Smash events dropped to a negligible 4.62%. These disjointed decision boundaries are visually corroborated by the confusion matrices in Figure 7. Specifically, GroupDRO (Figure 7e) shows substantial confusion between Background and Rain, while ProtoNet (Figure 7f) fails to establish a clear diagonal for the Smash class.

In contrast, the proposed DUPLE framework successfully mitigated these extreme disparities. DUPLE maintained balanced detection capabilities across all categories. Even on the most challenging Rain class, it retained a viable accuracy of 52.13%, a marked improvement over the near-zero failures observed in baseline methods. As illustrated in Figure 7(h), DUPLE recovers the diagonal structure of the confusion matrix, securing a consistent performance range of 52% to 69% across all four classes. This demonstrates that DUPLE prioritizes global reliability over peak performance on easier categories.

Analysis of OSDG2. Although the domain gap narrows on OSDG2, baseline models continued to exhibit distinct failure modes. Coral achieved perfect detection on Impact samples but sacrificed performance on the Climb class, where accuracy fell to 34.68%. Similarly, GroupDRO was heavily skewed, identifying 98.72% of Background samples but correctly classifying only 58.96% of Climb instances.

Among meta-learners, DUPLE demonstrated superior decision refinement. Quantitatively, DUPLE outperformed both GroupDRO and ProtoNet on the difficult Climb class with a leading accuracy of 86.41%, while maintaining strong performance on Background at 71.60% and Impact at 74.35%. The visual comparison between Figure 7(i) and Figure 7(l) further highlights this advantage: while GroupDRO misclassifies a significant portion of Impact samples as Background, DUPLE reduces this error and exhibits sharper diagonal dominance, indicating more precise decision boundaries.

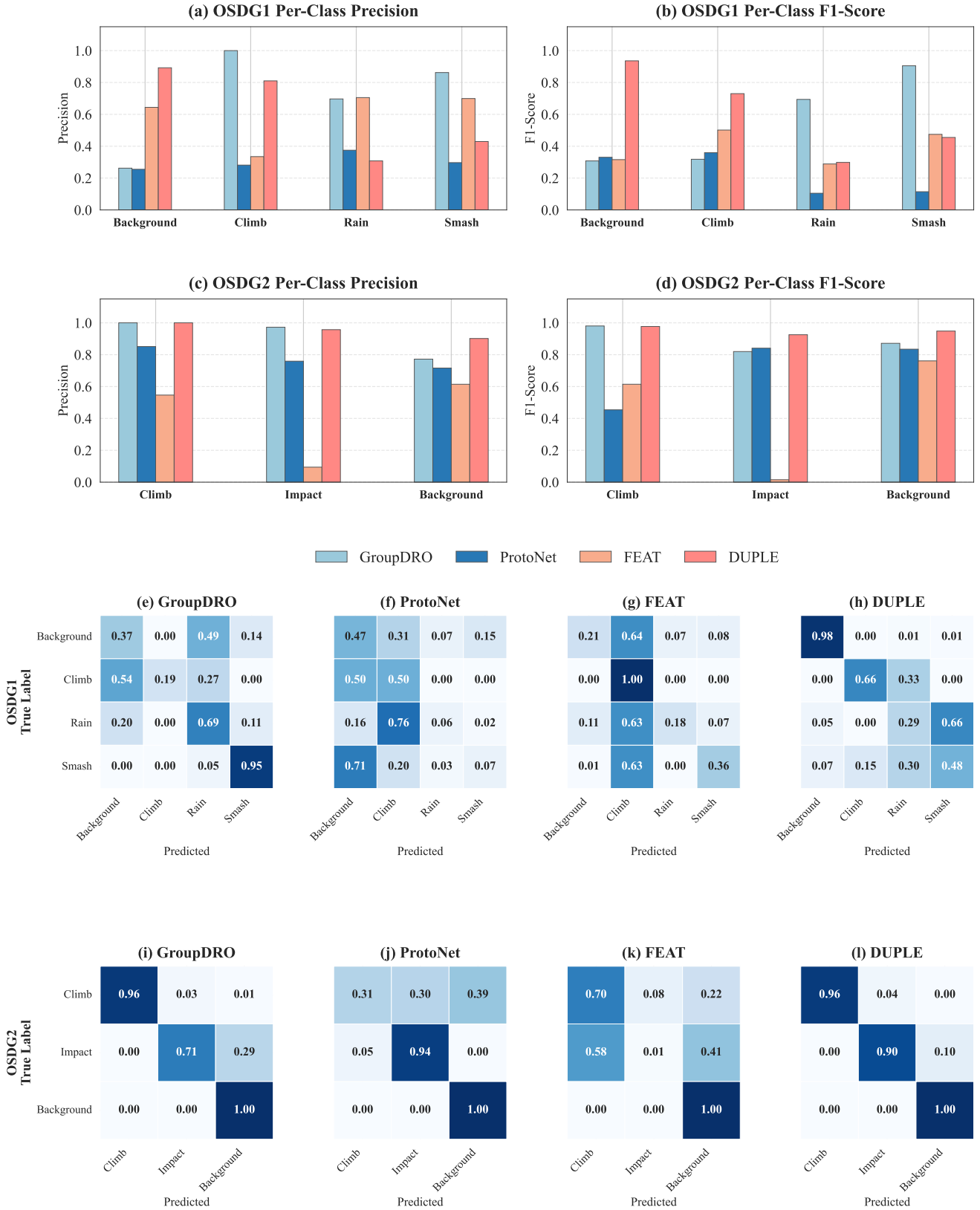


Figure 7: Per-class performance analysis on OSDG1 and OSDG2. (a-d) Precision and F1-scores. DUPL is compared against representative baselines: GroupDRO (DG), ProtoNet, and FEAT (Meta-learning). While GroupDRO outperforms standard baselines, it shows instability on challenging classes (e.g., Rain in OSDG1). DUPL (red) maintains robust performance across all categories. (e-l) Normalized confusion matrices. On OSDG1, GroupDRO (e) shows significant misclassification between Background and Rain. On OSDG2, GroupDRO (i) improves separation compared to metric-based methods like ProtoNet (j) but still confuses Impact with Background. DUPL (l) exhibits the sharpest diagonal structure, indicating effective adaptation to target domains.

Table 12: Per-Class Accuracy on OSDG1 and OSDG2.

Model	OSDG1				OSDG2		
	Background	Climb	Rain	Smash	Background	Climb	Impact
XGBoost	24.40 ± 24.40	67.04 ± 29.21	4.25 ± 3.44	38.37 ± 38.37	73.59 ± 37.35	56.50 ± 41.17	45.50 ± 41.32
SVM	9.60 ± 9.60	75.97 ± 14.72	43.92 ± 6.08	7.86 ± 7.86	63.16 ± 38.85	64.33 ± 45.58	39.17 ± 39.07
KNN	12.11 ± 4.11	3.72 ± 1.28	59.24 ± 8.07	64.60 ± 34.60	68.83 ± 31.03	39.06 ± 34.54	83.03 ± 17.46
1DCNN	0.00 ± 0.00	0.00 ± 0.00	63.94 ± 36.06	76.87 ± 17.41	28.67 ± 40.54	38.99 ± 37.88	87.67 ± 10.00
2DCNN	43.10 ± 38.30	59.46 ± 40.54	37.51 ± 30.78	41.63 ± 11.23	64.32 ± 41.77	44.69 ± 39.11	66.16 ± 46.78
LSTM	27.03 ± 27.03	32.56 ± 32.56	46.15 ± 46.15	16.53 ± 14.90	54.65 ± 40.19	43.92 ± 33.25	89.50 ± 13.46
Transformer	2.00 ± 1.20	42.01 ± 19.24	25.29 ± 0.29	42.43 ± 22.43	50.13 ± 8.57	70.32 ± 32.78	81.78 ± 15.63
GroupDRO	18.60 ± 18.60	58.83 ± 39.92	70.13 ± 1.02	64.03 ± 31.17	98.72 ± 1.81	58.96 ± 39.27	66.67 ± 47.14
Coral	11.63 ± 11.63	26.20 ± 22.45	70.66 ± 28.38	90.77 ± 3.63	78.52 ± 28.76	34.68 ± 45.50	100.00 ± 0.00
ProtoNet	59.25 ± 12.36	24.80 ± 24.80	37.52 ± 31.43	4.62 ± 2.47	51.65 ± 33.60	73.28 ± 15.32	74.56 ± 23.49
MAML	65.41 ± 29.01	61.46 ± 9.45	3.29 ± 0.15	28.95 ± 14.90	56.10 ± 22.56	59.41 ± 25.83	78.40 ± 23.72
ANIL	45.13 ± 24.69	39.36 ± 4.13	15.09 ± 5.73	41.77 ± 18.73	59.07 ± 38.61	61.95 ± 25.35	68.91 ± 32.57
R2D2	32.14 ± 20.66	84.75 ± 14.83	31.40 ± 5.66	12.68 ± 11.23	68.94 ± 29.44	58.28 ± 30.93	64.79 ± 12.28
FEAT	23.03 ± 2.10	65.06 ± 34.94	44.81 ± 26.66	66.49 ± 30.57	55.59 ± 32.83	42.45 ± 42.02	75.17 ± 35.11
<b>DUPLE (Ours)</b>	69.25 ± 29.14	64.87 ± 1.56	52.13 ± 23.19	65.99 ± 17.63	71.60 ± 36.82	86.41 ± 6.78	74.35 ± 19.37

In summary, the primary failure mode of baseline models across both datasets was single-class collapse caused by domain shift. DUPLE’s dual-domain statistically guided prototyping strategy effectively reduces this class-wise disparity, ensuring that performance remains viable even for the worst-case categories.

## 6. Conclusion

We present DUPLE, a prototype-based meta-learning framework for cross-deployment DFOS recognition under scarce target labels. The key idea is to construct deployment-tolerant class representations by exploiting complementary time–frequency evidence and adjusting predictions according to sample-specific statistics. Concretely, DUPLE (i) adopts multi-prototype representations to capture intra-class heterogeneity, (ii) infers domain reliability from raw statistical cues, and (iii) performs query-adaptive prototype aggregation at inference. Experiments on OSDG1 and OSDG2 show consistent improvements over strong baselines and, importantly, mitigate class-wise worst-case degradations under deployment shifts, leading to more dependable recognition across all activity categories. Ablation and analysis further verify that these design choices provide complementary gains rather than redundant complexity.

DUPLE achieves stable and state-of-the-art results on two cross-deployment benchmarks, OSDG1 and OSDG2. It not only improves overall accuracy but also precision, recall, and F1 score, and achieves more stable single-class performance compared to traditional classifiers, supervised deep networks, and robust meta-learning baseline models. These improvements stem from three synergistic factors: (i) dual-domain features capable of capturing complementary temporal and spectral cues; (ii) multi-prototype class representations covering heterogeneous patterns across different deployment environments; and (iii) query-aware aggregation guided by SGN, ensuring decision-making aligns with sample-specific statistics. These components

work together to achieve robust generalization under a context-domain generalization protocol, resulting in more stable and accurate model performance.

The limitation of this study lies in practical applications rather than the conceptual level; we focus only on single-event, single-channel scenarios. Extending DUPLE to multi-event recognition and multi-channel fusion is a logical next step. Nevertheless, the current results confirm that DUPLE is a powerful and deployment-robust baseline method for DFOS activity recognition.

## CRedit Authorship Contribution Statement

**Yifan He:** Conceptualization, Methodology, Software, Investigation, Data curation, Formal analysis, Visualization, Writing – original draft; **HaoDong Zhang:** Conceptualization, Methodology, Investigation, Writing – review & editing; **Qiheng Song:** Conceptualization, Resources; **Lin Lei:** Conceptualization, Data curation; **Zhenxuan Zeng:** Conceptualization, Writing – review & editing; **Haoyang He:** Investigation, Data curation; **Hongyan Wu:** Conceptualization, Methodology, Supervision, Writing – review & editing.

## Declaration of Competing Interest

Author Qiheng Song is a shareholder of Sichuan Fujinan Technology Co., Ltd., which provided the data used in this study. Sichuan Fujinan Technology Co., Ltd. had no role in the study design, data analysis, interpretation of the results, or the decision to submit the manuscript for publication. The other authors declare that they have no competing financial interests or personal relationships that could have influenced the work reported in this paper.

## Acknowledgments

The authors would like to thank Sichuan Fujinan Technology Co., Ltd. for providing the distributed fiber-optic sensing data and for their technical assistance with the experimental deployments.

## References

- Ajo-Franklin, J.B., Dou, S., Lindsey, N.J., Monga, I., Tracy, C., Robertson, M., Rodriguez Tribaldos, V., Ulrich, C., Freifeld, B., Daley, T., et al., 2019. Distributed acoustic sensing using dark fiber for near-surface characterization and broadband seismic event detection. *Scientific reports* 9, 1328.
- Allen, K., Shelhamer, E., Shin, H., Tenenbaum, J., 2019. Infinite mixture prototypes for few-shot learning, in: *International conference on machine learning*, PMLR. pp. 232–241.
- Bertinetto, L., Henriques, J.F., Torr, P.H., Vedaldi, A., 2018. Meta-learning with differentiable closed-form solvers. *arXiv preprint arXiv:1805.08136*.
- Chen, T., Guestrin, C., 2016. Xgboost: A scalable tree boosting system, in: *Proceedings of the 22nd acm sigkdd international conference on knowledge discovery and data mining*, pp. 785–794.
- Finn, C., Abbeel, P., Levine, S., 2017. Model-agnostic meta-learning for fast adaptation of deep networks, in: *International conference on machine learning*, PMLR. pp. 1126–1135.
- Hartog, A.H., 2017. *An introduction to distributed optical fibre sensors*. CRC press.
- He, Z., Liu, Q., 2021. Optical fiber distributed acoustic sensors: A review. *Journal of Lightwave Technology* 39, 3671–3686.
- Jia, H., Liang, S., Lou, S., Sheng, X., 2019a. A  $k$ -nearest neighbor algorithm-based near category support vector machine method for event identification of  $\phi$ -otdr. *IEEE Sensors Journal* 19, 3683–3689.
- Jia, H., Lou, S., Liang, S., Sheng, X., 2019b. Event identification by f-elm model for  $\Phi$ -OTDR fiber-optic distributed disturbance sensor. *IEEE Sensors Journal* 20, 1297–1305.
- Khaki, S., Wang, L., Archontoulis, S.V., 2020. A cnn-rnn framework for crop yield prediction. *Frontiers in Plant Science* 10, 1750.
- Lim, B., Arik, S.Ö., Loeff, N., Pfister, T., 2021. Temporal fusion transformers for interpretable multi-horizon time series forecasting. *International journal of forecasting* 37, 1748–1764.
- Lindsey, N.J., Dawe, T.C., Ajo-Franklin, J.B., 2019. Illuminating seafloor faults and ocean dynamics with dark fiber distributed acoustic sensing. *Science* 366, 1103–1107.
- Luong, H.V., Deligiannis, N., Wilhelm, R., Drapp, B., 2023. Few-shot classification with meta-learning for urban infrastructure monitoring using distributed acoustic sensing. *Sensors* 24, 49.
- Madsen, C., Bae, T., Snider, T., 2007. Intruder signature analysis from a phase-sensitive distributed fiber-optic perimeter sensor, in: *Fiber Optic Sensors and Applications V*, SPIE. pp. 141–148.
- Medsker, L.R., Jain, L., et al., 2001. Recurrent neural networks. *Design and applications* 5, 2.
- Muñoz, F., Soto, M.A., 2022. Enhancing fibre-optic distributed acoustic sensing capabilities with blind near-field array signal processing. *Nature Communications* 13, 4019.
- Qu, Z., Feng, H., Zeng, Z., Zhuge, J., Jin, S., 2010. A svm-based pipeline leakage detection and pre-warning system. *Measurement* 43, 513–519.
- Raghu, A., Raghu, M., Bengio, S., Vinyals, O., 2019. Rapid learning or feature reuse? towards understanding the effectiveness of maml. *arXiv preprint arXiv:1909.09157*.
- Rao, Y., Wang, Z., Wu, H., Ran, Z., Han, B., 2021. Recent advances in phase-sensitive optical time domain reflectometry ( $\Phi$ -OTDR). *photonic sensors* 11, 1–30.
- Sagawa, S., Koh, P.W., Hashimoto, T.B., Liang, P., 2019. Distributionally robust neural networks for group shifts: On the importance of regularization for worst-case generalization. *arXiv preprint arXiv:1911.08731*.
- Sherstinsky, A., 2020. Fundamentals of recurrent neural network (rnn) and long short-term memory (lstm) network. *Physica D: Nonlinear Phenomena* 404, 132306.
- Snell, J., Swersky, K., Zemel, R., 2017. Prototypical networks for few-shot learning. *Advances in neural information processing systems* 30.
- Sun, B., Saenko, K., 2016. Deep coral: Correlation alignment for deep domain adaptation, in: *European conference on computer vision*, Springer. pp. 443–450.
- Tejedor, J., Macias-Guarasa, J., Martins, H.F., Martin-Lopez, S., Gonzalez-Herraez, M., 2019. A contextual gmm-hmm smart fiber optic surveillance system for pipeline integrity threat detection. *Journal of Lightwave Technology* 37, 4514–4522.
- Tejedor, J., Macias-Guarasa, J., Martins, H.F., Piote, D., Pastor-Graells, J., Martin-Lopez, S., Corredera, P., Gonzalez-Herraez, M., 2017. A novel fiber optic based surveillance system for prevention of pipeline integrity threats. *Sensors* 17, 355.
- Titov, A., Kazei, V., AlDawood, A., Alfataierge, E., Bakulin, A., Osypov, K., 2022. Quantification of das vsp quality: Snr vs. log-based metrics. *Sensors* 22, 1027.

- Vaswani, A., Shazeer, N., Parmar, N., Uszkoreit, J., Jones, L., Gomez, A.N., Kaiser, Ł., Polosukhin, I., 2017. Attention is all you need. *Advances in neural information processing systems* 30.
- Vinyals, O., Blundell, C., Lillicrap, T., Wierstra, D., et al., 2016. Matching networks for one shot learning. *Advances in neural information processing systems* 29.
- Wang, J., Yang, Y., Mao, J., Huang, Z., Huang, C., Xu, W., 2016. Cnn-rnn: A unified framework for multi-label image classification, in: *Proceedings of the IEEE conference on computer vision and pattern recognition*, pp. 2285–2294.
- Wang, Z., Lu, B., Ye, Q., Cai, H., 2020. Recent progress in distributed fiber acoustic sensing with  $\Phi$ -OTDR. *Sensors* 20, 6594.
- Wu, H., Chen, J., Liu, X., Xiao, Y., Wang, M., Zheng, Y., Rao, Y., 2019a. One-dimensional cnn-based intelligent recognition of vibrations in pipeline monitoring with das. *Journal of Lightwave Technology* 37, 4359–4366.
- Wu, H., Gan, D., Xu, C., Liu, Y., Liu, X., Song, Y., Rao, Y., 2022. Improved generalization in signal identification with unsupervised spiking neuron networks for fiber-optic distributed acoustic sensor. *Journal of Lightwave Technology* 40, 3072–3083.
- Wu, H., Liu, X., Xiao, Y., Rao, Y., 2019b. A dynamic time sequence recognition and knowledge mining method based on the hidden markov models (hmm) for pipeline safety monitoring with  $\phi$ -otdr. *Journal of Lightwave Technology* 37, 4991–5000.
- Wu, H., Zhou, B., Zhu, K., Shang, C., Tam, H.Y., Lu, C., 2021. Pattern recognition in distributed fiber-optic acoustic sensor using an intensity and phase stacked convolutional neural network with data augmentation. *Optics express* 29, 3269–3283.
- Xu, C., Guan, J., Bao, M., Lu, J., Ye, W., 2017. Pattern recognition based on enhanced multifeature parameters for vibration events in  $\varphi$ -OTDR distributed optical fiber sensing system. *Microwave and Optical Technology Letters* 59, 3134–3141.
- Xu, C., Guan, J., Bao, M., Lu, J., Ye, W., 2018. Pattern recognition based on time-frequency analysis and convolutional neural networks for vibrational events in  $\varphi$ -otdr. *Optical Engineering* 57, 016103–016103.
- Ye, H.J., Hu, H., Zhan, D.C., Sha, F., 2020. Few-shot learning via embedding adaptation with set-to-set functions, in: *Proceedings of the IEEE/CVF conference on computer vision and pattern recognition*, pp. 8808–8817.
- Zhang, H., Gao, J., Hong, B., 2022.  $\phi$ -otdr signal identification method based on multimodal fusion. *Sensors* 22, 8795.
- Zhong, R., Chiang, C.Y., Jaber, M., De Wilde, R., Hayward, P., 2025. Intelligent travel activity monitoring: Generalized distributed acoustic sensing approaches. *arXiv preprint arXiv:2506.10237*.
- Zhou, H., Zhang, S., Peng, J., Zhang, S., Li, J., Xiong, H., Zhang, W., 2021. Informer: Beyond efficient transformer for long sequence time-series forecasting, in: *Proceedings of the AAAI conference on artificial intelligence*, pp. 11106–11115.